On Process, Structure, Property Relationships in Impact Welding of Aluminum 6061 and Steel 4130

Yu Mao[1], V. Gupta[2], B. Ufferman[1], A. Vivek[1*], K. S. Choi[2], X. Sun[3], G. S. Daehn[1]

[1] Department of Materials Science and Engineering, The Ohio State University, USA
[2] Pacific Northwest National Laboratory, USA
[3] Oak Ridge National Laboratory, USA
*Corresponding author. Email: vivek.4@osu.edu

Abstract

Vaporizing Foil Actuator Welding process was used to weld 1mm thick aluminum alloy 6061 sheet to 3.2 mm thick 4130 grade steel plate. Temporal evolution of the flyer sheet velocity was recorded at four locations on the flyer sheet using photonic Doppler velocimetry. The welded samples were subjected to mechanical and microstructural characterization. Although the welded interface did not show a very wavy characteristic, the welds had substantial strength. Welds made with a softer temper, T4 alloy were found to be stronger than the one created with a harder, T6 temper alloy. A coupled Lagrangian-Eulerian numerical framework was also utilized to predict the structure of the interface based on the measured velocity profile. The model also depicted absence of large waves although the jetting phenomenon was observed, thereby providing insight into necessary conditions for impact welding.

Keywords

VFAW, wavy interface, coupled Lagrangian-Eulerian modeling

1 Introduction

For the past few decades, government mandates have pushed automotive manufacturers to increase the fuel efficiency of their vehicles (Bento et al., 2015). One of the main strategies used to achieve this goal is by reducing the weight of vehicles, for example by substituting aluminum for steel. The issue with this transition is that it requires

different joining methods than resistance spot welding used for traditional steel to steel joints since fusion welding steel to aluminum leads to the formation of brittle intermetallic compounds (Meschut et al., 2014). Two alternate methods of joining these types of materials are mechanical fasteners and adhesive bonding. Mechanical fasteners add weight to the system and introduce galvanic couples that pose corrosion issues (Meschut et al., 2014) and (Martinsen, 2015). Adhesives are difficult to handle and have to be cured for tens of minutes to obtain structural strength from them (Martinsen, 2015). However, adhesives do offer a solution to the galvanic corrosion problem in multi-material joints, and are getting increasingly utilized in body-in-white assembly (Skszek et al., 2015)

Vaporizing Foil Actuator Welding, an impact welding process offers an alternative to fasteners due to its ability to weld dissimilar materials without melting (Vivek et al., 2013). In this method, a large electrical current is passed through a thin aluminum foil. The electrical current causes the aluminum to rapidly vaporize, generating a large pressure pulse that drives the two sheets of metal to be joined together at a speed of at least 300 m/s. During impact, surface oxide layers are scoured off by a jetting mechanism, which enables metallic bonding directly between the two metals. An added benefit of VFAW as compared to explosive welding is that it is amenable to future automation and similar in scale to resistance spot welding. Compared to Magnetic Pulse Welding (MPW), VFAW offers a better energy conversion efficiency (Hahn et al., 2016) and does not suffer from the issue of coil longevity (Golovashchenko, 2007)

The quality and strength of the joint obtained in the VFAW process is heavily dependent on the input process parameters, geometric configuration, and the materials involved. A predictive simulation capability can help in identifying the optimal process conditions that will result in a robust joint. The conventional finite element method (FEM) framework based on purely Lagrangian formulation is not suitable to model the impact owing to the mesh distortion problems due to large deformation of the material at the weld interface. With the rapid advancement of computational techniques in last two decades, several researchers have shown success in capturing the complex wavy interfacial structure through computational simulations. These simulation frameworks utilized different formulations including Eulerian (Mousavi and Al-Hassani, 2005), (Grignon et al., 2004), and (Raoelison et al., 2016), Arbitrary Lagrangian-Eulerian (ALE) (Nassiri et al., 2015), and Smoothed Particle Hydrodynamics (SPH) (Wang et al., 2012), and (Nassiri et al. 2017). An Eulerian formulation based approach is developed in this work to simulate the impact between the steel and aluminum plates. The model predicts the interfacial structure and the temperature distribution in the metal sheets.

The predictive model developed here is validated against experimental data from welding of aluminum and steel alloys with known high-strain rate constitutive data. In addition, the conditions for formation of strong and weak bonds are also determined, and the dependence of weld strength on characteristic interface waviness and jet formation is also tested.

2 Procedure

2.1 Experimental

The flyer was 1 mm thick Al6061 and a 3.175 mm thick 4130 steel sheet was used as the target. In order to adapt to the Johnson-Cook strength and damage coefficients obtained by previous research (Wuertemberger and Palazotto, 2016) the 4130 steel was normalized by austenitizing above 910 °C. The steel was subsequently water quenched and then tempered at 566 °C until strength was between 827-965 MPa, and hardness was between 24-30 HRC. Al6061 was received in full-hard T6 condition and Al6061-T4 sheets were obtained by annealing the T6 material at 532 °C, water quenching, and then natural aging at room temperature for 24 hours.

The geometry of both patch and spot foils used as the actuators are shown in Figure 1. All foils were 1.27 mm thick and made from 3003 Al. G10 sheets that were 1.5 mm thick were the standoffs, which were positioned parallel to the length of the foil.

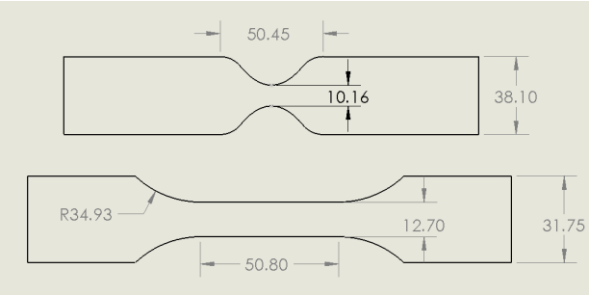

Figure 1: Dimensions of the spot foil (top) and patch foil (bottom). Dimensions are in mm.

The separation between the standoffs was equivalent to the width of the foil – 38.1 mm for spot configuration and 31.75 mm for patch configuration. The schematic of a VFAW setup is shown in Figure 2. Before welding, the faying surfaces of flyers and targets were ground with 50 grit sandpaper then cleaned using acetone. Spot welds of Al6061-T6 and Al6061-T4 to 4130 steel were made at the energy level of 6 kJ. Patch welds of Al6061-T6 and Al6061-T4 to 4130 steel were made at the energy level of 10kJ.

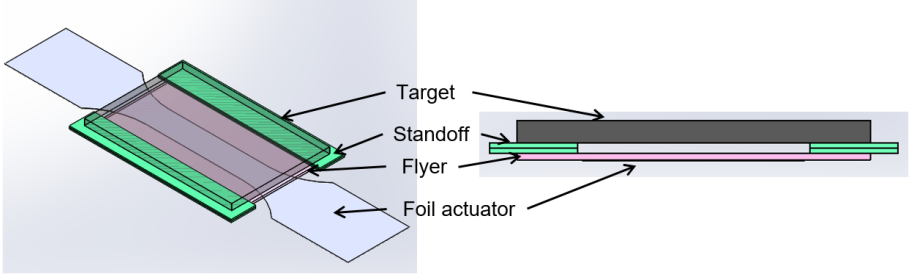

Figure 2: Schematic of VFAW using patch foil

Photonic Doppler Velocimetry (PDV) experiments were performed to obtain the velocity of the flyer during the welding process. Velocity Interferometer System for Any

Reflector (VISAR), introduced by Barker and Hollenbach (1972), was a widely-used tool to measure the velocity of high speed targets. PDV is a more contemporary method utilizing readily available telecommunications devices (Vivek et al., 2014a). During the PDV experiments, the 4130 steel target was replaced by a transparent polycarbonate plate, and the PDV probe was oriented perpendicular to the surface of the traveling aluminum flyer.

Lap shear tests were performed to determine the strength of the welds. All tests were conducted on a MTS tensile machine at a cross-head speed of 0.1 mm/s. Optical microscopic characterization was performed to observe the welding interface. The weld was sectioned, mounted, and polished prior to performing optical microscopy.

2.2 Simulation

Figure 3 depicts the VFAW process and shapes of welds possible with it. The schematic in Figure 3(C) illustrates the welding event at a cross-section across the width of the weld specimen. The impact between the base plate and flyer leading up to the joint interface is modelled here to gain insight into the dynamic process. In a typical Lagrangian formulation based finite element simulation of the high speed impact process, the severe plastic deformation at the weld interface causes excessive mesh distortion that lead to numerical instabilities. Therefore, to overcome this problem, a finite element model based on the Coupled Eulerian Lagrangian (CEL) formulation is developed to simulate the high-speed impact between aluminum and steel sheets. The simulation framework is developed in the commercial finite element software ABAQUS/Explicit (Abaqus 6.13 Documentation, 2013).

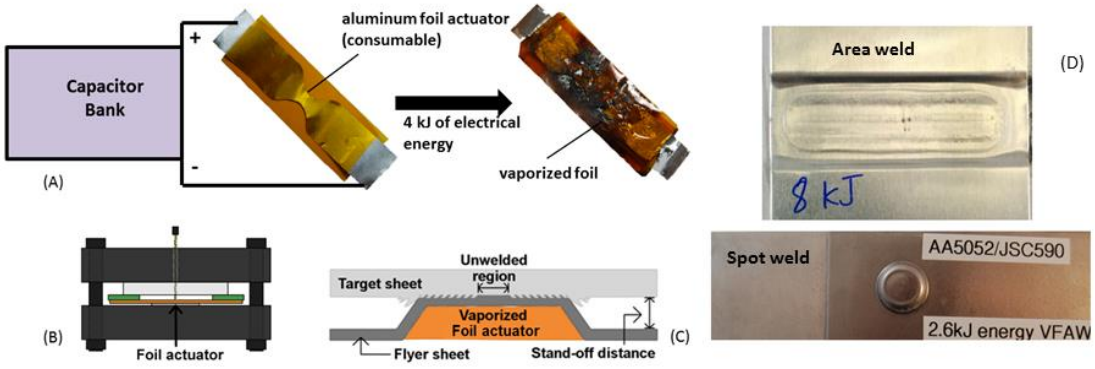

Figure 3: Schematics of VFAW: (A) Foil consumable, before and after being used, (B) typical welding assembly, (C) welding event, and (D) different weld geometries possible with various foil actuator shapes.

As can be seen from Figure 3(C), there is symmetry in the geometric configuration and loading about a plane passing through the half-width point. Therefore, only half of this configuration is considered in the model, and symmetry boundary conditions are applied to account for the deformation constraints from the rest of the system. The finite element

model requires prescribing either the initial conditions or the forcing boundary conditions that govern the motion of flyer, and result in realistic impact conditions. Most of the work reported in literature on modeling the impact welding process assume a constant impact angle, and assign uniform velocity to the flyer (Nassiri et al., 2017), (Mousavi et al., 2005), and (Nassiri et al., 2015), or utilize an analytical function to define the velocity distribution along the length of the flyer (Raoelison et al., 2016), and (Xu and Sun, 2015). These assumptions might be reasonable for certain weld set-ups, but do not capture the dynamic impact angle along the width of the weld, resulting from the bending deformation of flyer in the current set up. In the model, prescribing velocity (or displacement) at specific points of the flyer will constrain the deformation of the flyer leading to unrealistic impact conditions at the interface. Therefore, it is important that the model accurately captures the deformation and velocity response of the flyer plate for at least the width of weld. As described in Section 2.1, the velocity histories for different points along the length of the flyer are measured during the experiments using PDV. In the VFAW process, these velocities are the response of the flyer due to the pressure exerted on it by the expanding vapors.

Due to lack of any in-situ pressure measurements in the welding experiment, an inverse approach was used to determine a pressure profile and resulting velocity history that matches the velocity measurements made during the experiments using PDV. The schematic in Figure 4 illustrates the location of the spots where PDV measurements were made. A pressure was applied at the bottom surface of the flyer to cause motion of the flyer. In this approach, the pressure profile is an input to the model and the velocity history at the points corresponding to the locations for which PDV data is available is considered as the output. Several different polynomial pressure profiles were iterated upon, until a reasonable match in the velocity history was obtained between the experimental measurements and the simulation results. For the simulations carried out in this exercise, a pure Lagrangian approach was adopted since it only involved the deformation of the flyer. This also enabled the collision with the target to be omitted. The pressure profile determined by this trial and error approach is shown in Figure 6, and is a combination of uniform pressure between Spot 1 and Spot 2, and a cubic profile from spot 2 onwards up to a certain distance obtained iteratively.

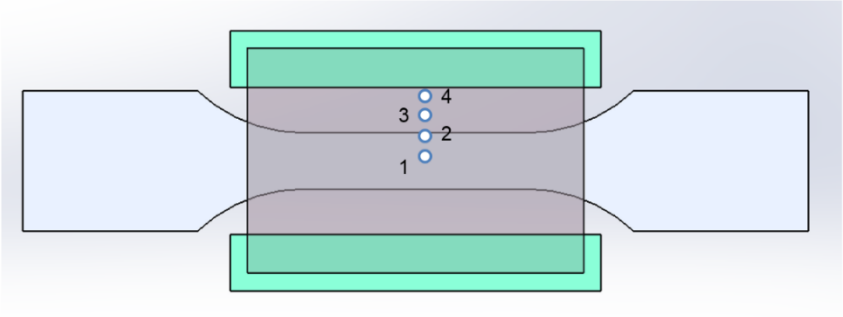

Figure 4: Illustration of the weld configuration showing the location of spots for velocity measurements. Spot 1 is at the center of the foil width, and each next subsequent spot is located at 3.81 mm.

Figure 5 shows the CEL model set-up and the boundary conditions applied to the system. The stand-off and anvil are modelled as Lagrangian bodies which are fixed in space. Any out-of-plane movement of the material is restricted. The initial configurations of flyer and target are modeled by assigning volume fraction of the corresponding material in the Eulerian mesh. For example, in the region of target, an initial volume fraction of 1.0 for steel is assigned. The contact interaction between the Lagrangian bodies and the Eulerian materials is defined using the general contact in Abaqus (Abaqus 6.13 Documentation, 2013). The Eulerian method in Abaqus is only implemented for the three-dimensional elements, therefore, a small and arbitrary model thickness of 0.02 mm is chosen in the z-direction. For dissipation of heat through the system, a reasonable boundary condition in the form of convection is defined at the bottom face of the Eulerian domain with a uniform convective coefficient of 0.3 W/m^2 K and sink temperature of 298 K. All other surfaces are assumed to be insulated. Due to the transient nature of the high-speed impact process, the thermal boundary conditions should not influence the peak temperature predictions at the weld interface. The plastic flow behavior of the materials under high strain rate and elevated temperature is accounted for by using the Johnson-Cook material model (Johnson, 1983). The parameters used for the model are from (Vedantam et al., 2006) for steel and (Lesuer et al., 2001) for aluminum.

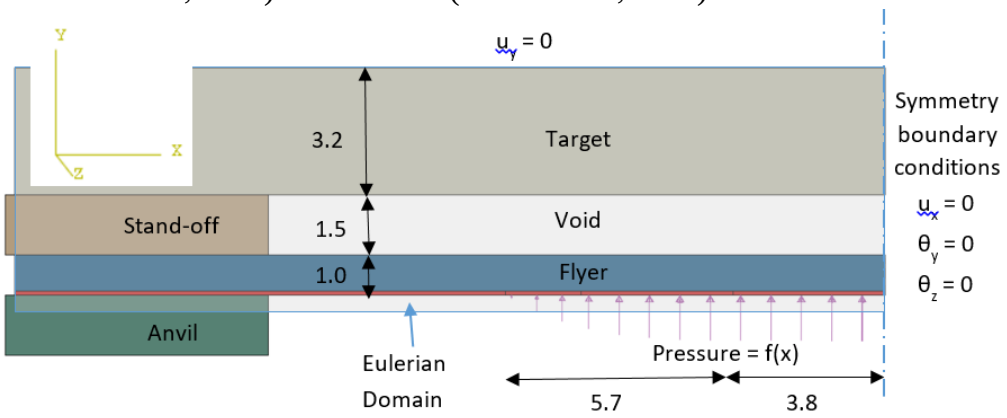

Figure 5: CEL model set-up for the weld configuration. All the dimensions are in mm.

It is noted that the velocity history obtained from the simulation continues to rise beyond 2 μs, since there is no target plate in this simulation. The choice of this pressure profile is not unique, and other functional forms for the spatial variation of the pressure can be considered as well. The chosen profile, which is a combination of uniform and cubic distribution in the two different portions of the flyer length, is one choice and partially inferred by observing the experimental PDV data. As can be seen from Figure 6, the experimentally measured velocity history at spots 1 and 2 overlay on top of each other, and hence the choice of uniform pressure distribution between the two spots. Attempts were not made to match the velocity data from Spot 4 because that may require temporal variation in the pressure profile and moreover, the weld interface does not extend that far from the center.

There is an inherent issue in this kind of Eulerian representation of material. There is no straightforward way in Abaqus to prescribe force boundary conditions on the material boundary, since the material is not tied to the mesh, unlike the pure Lagrangian approach. To circumvent this issue, a thin strip of material (0.1 mm thickness) at the bottom of the flyer is defined as a Lagrangian body, so that the pressure boundary conditions can be applied to drive the motion of the flyer. The interaction between the thin Lagrangian strip and rest of the Eulerian flyer is defined using the general contact. It is understood that such a set-up of splitting a continuum component into Lagrangian and Eulerian representation would lead to unrealistic deformation and stress field near the contact surface between the two material representations. However, this should not have any significant influence on the deformation field at the weld interface, which is the region of interest.

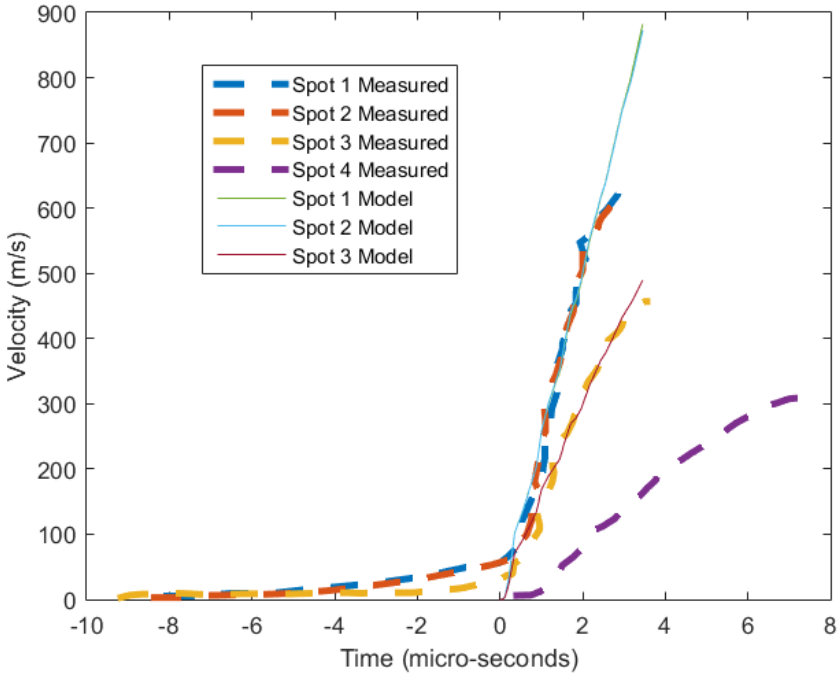

Figure 6: Experimentally measured velocity history and simulated output for velocities at different points along the length of the flyer.

3 Results and Discussion

3.1 Interface structure

Optical images of waviness within the patch weld of Al6061-T6 and spot weld of Al6061-T6 and T4 to 4130 steel are shown in Figures 7 and 8. Small amplitude waves are observed at the interface of a patch weld in Figures 7c and d. There is typically a discontinuous layer between the target and flyer along the wavy interface, which is widely believed to be intermetallic compounds of aluminum and steel (IMC) (Vivek et al., 2014b). As shown in Figure 7, spot welds yield relatively higher amplitude waves due to higher impact velocity. There is no significant difference in degree of waviness between aluminum flyers of T4

and T6 conditions. However, compared with explosive welding, the waviness of the weld created by VFAW, which has a wavelength on the order of 100 μm, is still not as large (Szecket et al., 1985). Figure 8 shows a full symmetric view of the joining interface of Al 6061-T6 in the spot weld configuration, indicating the existence of an unwelded region at the center due to the inadequate collision angle at impact, and the severe rebound afterwards. A continuous layer of IMC formed on both sides just outside of the central unwelded region as a result of low impact angle and high impact velocity (Vivek et al., 2014b), as shown in Figure 8c. The IMCs are typically brittle and therefore fractured after welding.

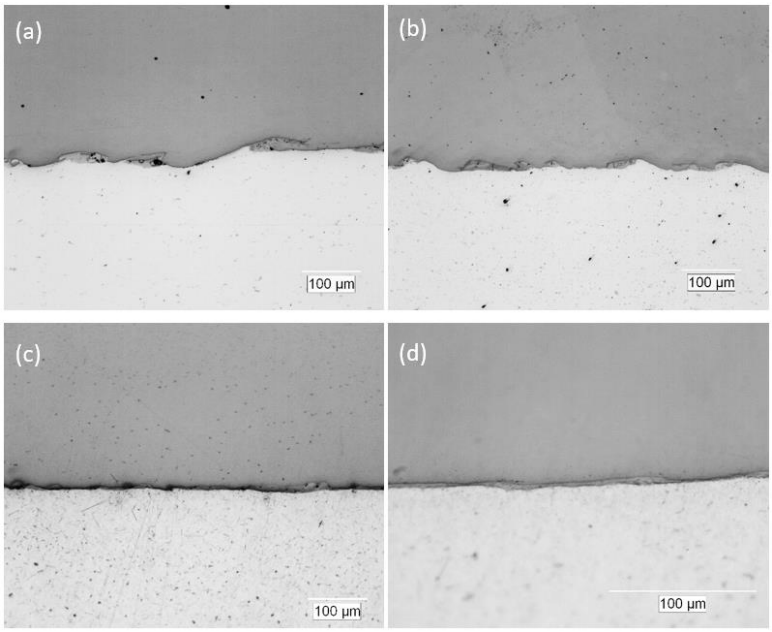

Figure 7: Waviness observed at interface cross section of spot weld of Al 6061-T6 (a) and Al 6061-T4 (b) and patch weld of Al 6061-T6 (c) and Al 6061-T4 (d) to 4130 steel. IMC formed in state of small pockets in spot welds of both conditions and continuous layer in patch weld of T6 condition.

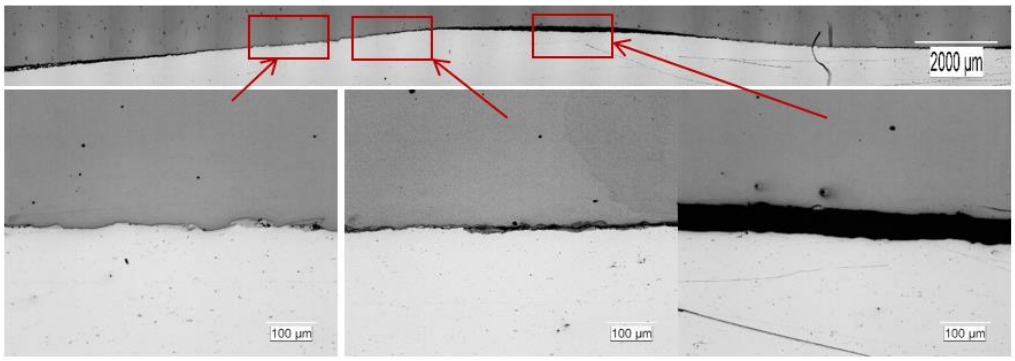

Figure 8: Interface cross section of spot weld of Al 6061-T6 to 4130 steel (a). Welded regions of waviness lie on two sides of the unwelded region at the center, connected by regions of fractured layer of IMC in between.

The finite element simulation for the weld process was carried out using the model described in Section 2.2. The 8-node (hexahedral) trilinear temperature and displacement elements were used to mesh the domain with a uniform element size of 10 μm. Figure 9: Deformation of the flyer and interfacial structure: Contour plot represents the volume fraction of flyer material (Al 6061-T6).\9 shows the instantaneous contour plot for the volume fraction of aluminum at t = 4.4 μs, capturing the flyer deformation and the resulting weld interface structure. As the weld progresses away from the center towards the ends, the impact angle increases, and enables jetting in front of the collision front. The jetting provides cleaned, oxide-free faying surfaces. This allows atomic contact between the two metal surfaces, causing the formation of a metallic bond. The distinct wavy interfacial structure, which is typically associated with impact welding, is not observed for this welding condition. This is in agreement with the micrograph of the weld-cross-section obtained experimentally and shown in figures 7c, 7d, and 8.

Figure 10: Temperature prediction in the weld interface region. Values for the contour bar are in degree Kelvin.10 provides the instantaneous temperature distribution in the weld interface region predicted from the simulation. The upper limit for the contour bar is set to the melting point temperature for Al 6061 (926 K). The thin grey region along the interface indicates melting of the aluminum flyer.

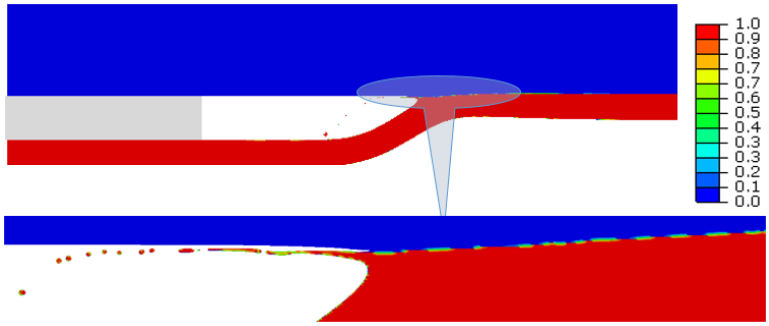

Figure 9: Deformation of the flyer and interfacial structure: Contour plot represents the volume fraction of flyer material (Al 6061-T6).\

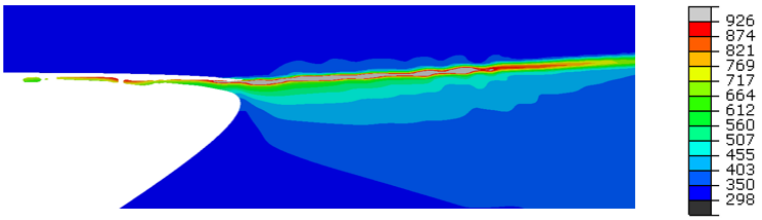

Figure 10: Temperature prediction in the weld interface region. Values for the contour bar are in degree Kelvin.

A similar approach was taken to simulate the impact in the spot weld configuration, which results in higher impact velocity compared to the patch configuration. In this configuration, the velocity data from PDV is obtained at the two spots indicated in Figure 11: Spot weld configuration showing the locations of spots where velocities were measured using PDV.11. A cubic pressure profile provides a reasonable match between the experimentally

measured and simulated velocity output (Figure 12: Experimentally measured velocity history and simulation output in spot configuration.12).

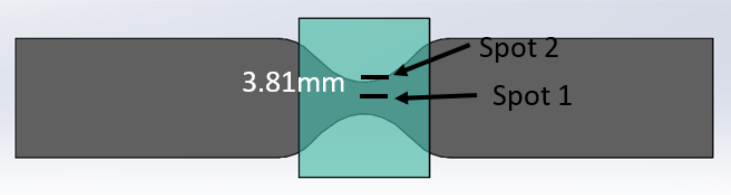

Figure 11: Spot weld configuration showing the locations of spots where velocities were measured using PDV.

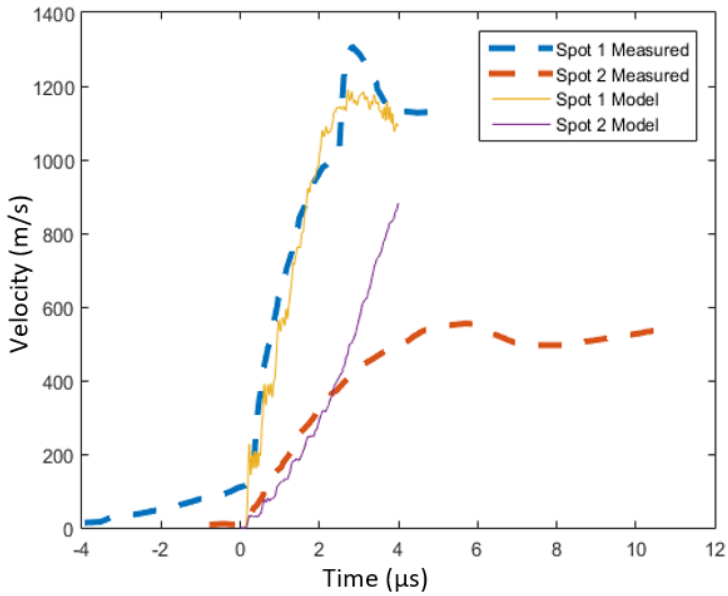

Figure 12: Experimentally measured velocity history and simulation output in spot configuration.

Figure 9: Deformation of the flyer and interfacial structure: Contour plot represents the volume fraction of flyer material (Al 6061-T6).\3 shows the instantaneous contour plot for the volume fraction of aluminum at t = 3.0 μs, capturing the flyer deformation and the jetting. In this configuration, the jetting seems to start closer to the center as compared to the patch configuration. This is attributed to the fact that for any given point located a certain distance from the center, the spot configuration results in higher impact velocity and angle compared to the patch configuration. This also explains the larger ratio of un-welded to welded region for the patch configuration.

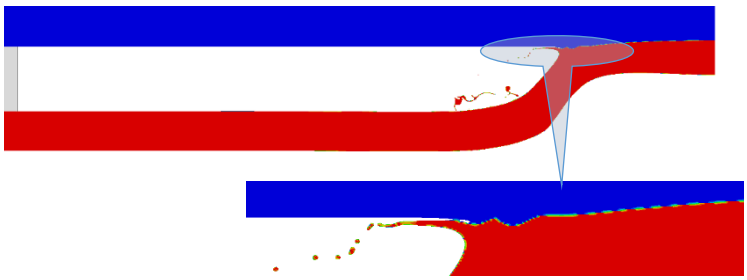

Figure 13: Deformation of the flyer and depiction of jetting in the spot configuration.

3.2 Mechanical properties

Patch and spot welds as welded and after lap shear testing are shown in Figures 14 and 15, respectively. Lap shear testing data for the spot weld configuration are shown in Figure 16. For patch welds, there is a dramatic difference between Al 6061 flyers in T4 and T6 conditions in both failure mode and failure load. All welds made with the T6 flyer failed at the interface, shown in Figure 14c. The failure load for most samples was below 1.5 kN. There is high uncertainty in the accuracy of the data since this value is close to the lower detection limit and resolution of the testing equipment. In comparison, all the T4 welds failed through the Al6061 flyer, as shown in Figure 14b, with a failure load of approximately 15kN. For spot welds, welds of aluminum in both conditions were strong enough to yield base metal failure during lap shear testing, shown in Figure 15. Therefore, the higher peak load and lower elongation in T6 than T4 shown in Figure 16 is consistent with the initial different mechanical properties of Al6061 in those two tempers. The failure mode of T4 during pry testing was nugget tear out, while it was interfacial for T6, as shown in Figure 17. According to the welded area of the samples in T6 condition after pry testing, the minimum shear strength of the weld is calculated to be 42.38 MPa which is acceptable; the unwelded zone at the center is also observed.

The results from mechanical tests are consistent with the microscopic observation. The state of IMC plays an important role in determining the strength of the weld. The continuous layer of IMC in T6 patch weld greatly weakens the strength. Despite a flat interface in the spot weld of both T4 and T6 conditions, the welds have good strength with IMC in the state of discontinuous pockets. This further indicates that waviness is not critical for joint strength of aluminum-steel impact weld.

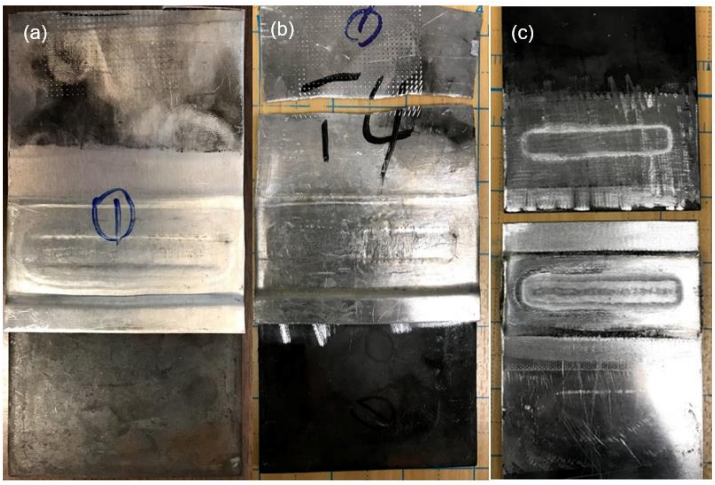

Figure 14: Patch weld of Al6061 to 4130 steel as welded (a), Al 6061-T4 as flyer (b) and Al 6061-T6 as flyer after lap shear test (c). The weld failed in different modes during test for the two cases.

Figure 15: Spot weld of Al6061-T6 to 4130 steel as welded (a) and after lap shear test (b). Aluminum flyer failed during test for both cases of T4 and T6.

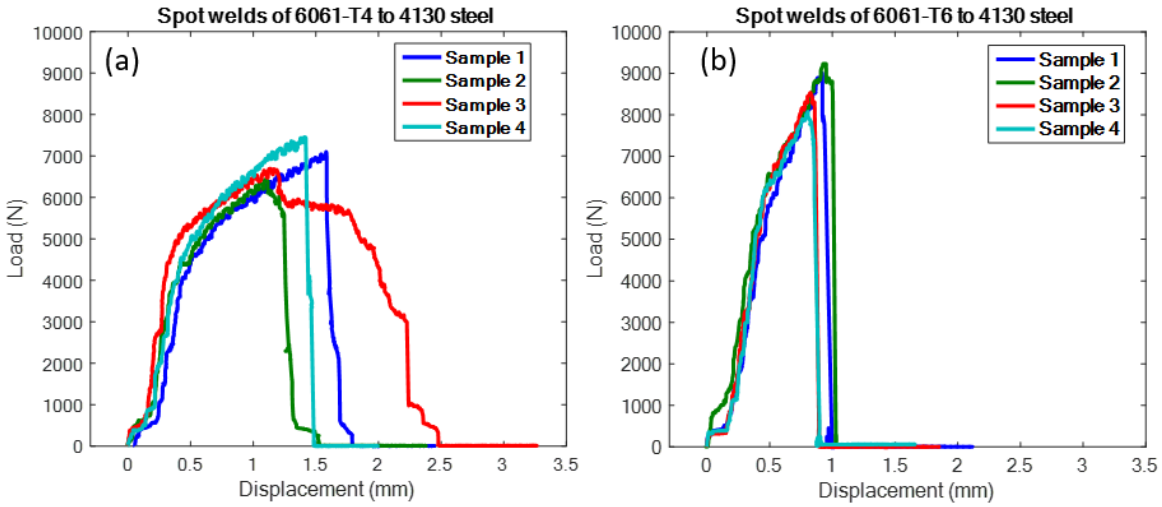

Figure 16: Lap shear test results of spot welds of 6061-T4 (a) and 6061-T6 (b)

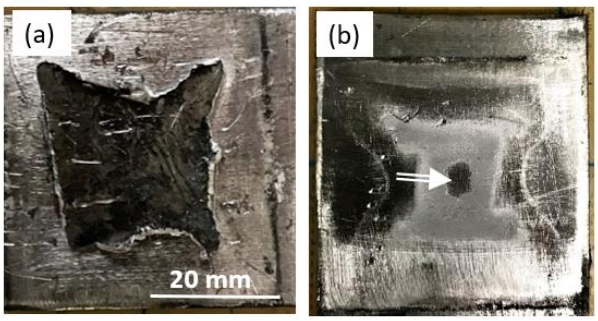

Figure 17: Spot welds of 6061-T4 (a) and 6061-T4 (b) to 4130 steel after pry test. T4 condition failed a nugget and T6 condition was peeled off leaving a hint of welding. The arrow in (b) represents the unwelded region found in the center of the spot weld.

4 Conclusions

Based on the micrographs of sectioned welds and the results of the various simulations, the presence of waviness often associated with impact welding is not a requirement to attain a high strength joint. Jetting of the surface oxides and contaminants, though, does seem to be an essential process to achieve a high quality VFAW joint. Most micrographs presented show discontinuous pockets of IMCs. Therefore, the presence of IMCs is not deleterious to the joint strength so long as they do not form a continuous layer along the interface. For patch welds, Al 6061 in T4 condition creates significantly stronger welds than T6 condition. Given the identical chemical composition and impact parameters, the distinction in mechanical properties is likely responsible for their different mechanical responses. Both Al 6061-T4 and T6 create spot welds of good quality that are stronger than the base aluminum. The coupled Lagragian-Eulerian numerical formulation based simulation framework gives outputs that are consistent with experimental results, and therefore is validated to predict the structure of the welded interfaces.

4.1 Acknowledgments

This work was funded by the U.S. Department of Energy (DOE) Award No. DE-EE0007813. The authors are also thankful to Ohio Supercomputing Center for providing high-performance computing support.

References

2013, *Abaqus 6.13 Documentation*. Dassault Systems Ivχ Providence, RI, USA.

Barker, L.M., Hollenbach, R.E., 1972. *Laser interferometer for measuring high velocities of any reflecting surface.* Journal of Applied Physics 43 (11), pp. 4669-4675.

Bento, A., Roth, K., Wang, Y., 2015. *The Impact of CAFE Standards on Innovation in the US Automobile Industry.* In: AAEA & WAEA Joint Annual Meeting, San Francisco, California, USA.

Grignon, F., Benson, D., Vecchio, K.S., Meyers, M.A., 2004. *Explosive welding of aluminum to aluminum: analysis computations and experiments*, International Journal of Impact Engineering 30 (10), pp. 1333-1351.

Golovashchenko, S.F., 2007. Material formability and coil design in electromagnetic forming. *Journal of Materials Engineering and Performance*, *16*(3), pp.314-320.

Lesuer, D.R., Kay, G.J., LeBlanc, M.M., 2001. *Modeling large-strain, high-rate deformation in metals.* In: Third Biennial Tri-Laboratory Engineering Conference Modeling and Simulation, pp. 3-5.

Hahn, M., Weddeling, C., Taber, T., Vivek, A., Daehn, G.S., Tekkaya, A.E., 2016. *Vaporizing foil actuator welding as a competing technology to magnetic pulse welding.* Journal of Materials Procesing Technology 230, pp. 8-20.

Johnson, G.R., 1983. *A constitutive model and data for metals subjected to large strains, high strain rates and high temperatures.* In: 7th International Symposium on Ballistics, Hague, Netherlands.

Martinsen, K., Hu, S.J., Carlson, B.E., 2015. *Joining of dissimilar materials.* CIRP Annals - Manufacturing Technology 64, pp. 679–699.

Meschut, G., Janzen, V., Olfermann, T., 2014. *Innovative and Highly Productive Joining Technologies for Multi-Material Lightweight Car Body Structures.* Journal of Materials Engineering and Performance 23 (5), pp. 1515–1523.

Mousavi, A.A.A., Al-Hassani, S.T.S., 2005. *Numerical and experimental studies of the mechanism of the wavy interface formations in explosive/impact welding*. Journal of Mechanics and Physics of Solids 53, pp. 2501-2528.

Mousavi, A.A.A., Burley, S.J., Al-Hassani, S.T.S. 2005. *Simulation of explosive welding using the Williamsburg equation of state to model low detonation velocity explosives.* International Journal of Impact Engineering 31, pp. 719-734.

Nassiri, A., Chini, G., Vivek, A., Daehn, G.S., Kinsey, B., 2015. *Arbitrary Lagrangian-Eulerian finite element simulation and experimental investigation of wavy interfacial morphology during high velocity impact welding.* Materials & Design 88, pp. 345-358.

Nassiri, A., Vivek, A., Abke, T., Liu, B., Lee, T., Daehn, G.S., 2017. *Depiction of interfacial morphology in impact welded Ti/Cu bimetallic systems using smoothed particle hydrodynamics.* Applied Physics Letters 110, pp. 231601-1-213601-5.

Raoelison, R.N., Sapanathan, T., Padayodi, E., Buiron, N., Rachik, M., 2016. *Interfacial kinematics and governing mechanisms under the influence of high strain rate impact conditions: Numerical computations of experimental observations.* Journal of the Mechanics and Physics of Solids 96, pp. 147-161.

Skszek, T.W., Zaluzec, M., Conklin, J. and Wagner, D., 2015. *MMLV: project overview* (No. 2015-01-0407). SAE Technical Paper.

Szecket, A., Inal, O.T., Vigueras, D.J., Rocco, J., 1985. *A wavy versus straight interface in the explosive welding of aluminum to steel.* Journal of Vacuum Science and Technology A: Vacuum, Surfaces, and Films 3 (6), pp. 2588-2593.

Vedantam, K., Bajaj, D., Brar, N.S., Hill, S., 2006. *Johnson-Cook strength models for mild and DP 590 steels*. In: AIP Conference Proceedings, pp. 775-778.

Vivek, A., Hansen, S.R., Liu, B.C. and Daehn, G.S., 2013. Vaporizing foil actuator: A tool for collision welding. *Journal of Materials Processing Technology*, *213*(12), pp.2304-2311.

Vivek, A., Hansen, S.R., Daehn, G.S., 2014a. *High strain rate metalworking with vaporizing foil actuator: Control of flyer velocity by varying input energy and foil thickness*. Review of Scientific Instruments 85 (7), pp. 075101-1-075101-8.

Vivek, A., Liu, B.C., Hansen, S.R., Daehn, G.S., 2014b. *Accessing collision welding process window for titanium/copper welds with vaporizing foil actuators and grooved targets.* Journal of Materials Processing Technology 214 (8), pp. 1583-1589.

Wang X., Zheng, Y., Liu, H., Shen, Z., Hu, Y., Li, W., Gao, Y., Guo, C., 2012. *Numerical study of the mechanism of explosive/impact welding using Smoothed Particle Hydrodynamics method*. Materials & Design 35, pp. 210-219.

Wuertemberger, L., Palazotto, A.N., 2016. *Evaluation of flow and failure properties of treated 4130 steel.* Journal of Dynamic Behavior of Materials 2 (2), pp. 207-

222.Xu, W., Sun, X., 2015. *Numerical investigation of electromagnetic pulse welded interfaces between dissimilar metals.* Science and Technology of Welding and Joining 1718, p. 1362171815Y.000.